

Dao Huy Bich · Dinh Gia Ninh

# Research on dynamical buckling of imperfect stiffened three-layered toroidal shell segments containing fluid under mechanical loads

Received: 17 June 2016 / Published online: 11 October 2016  
© Springer-Verlag Wien 2016

**Abstract** An analytical approach to the nonlinear dynamical buckling of imperfect stiffened three-layered toroidal shell segments containing fluid is performed in this paper. The toroidal shell segments are reinforced by ring and stringer stiffeners system in which the material properties of the shell are assumed to be continuously graded in the thickness direction. Based on the classical thin shell theory with geometrical nonlinearity in von Karman–Donnell sense, Stein and McElman assumption, theoretical formulations are derived with the smeared stiffeners technique. Furthermore, the dynamical pressure of the fluid is taken into account. The fluid is assumed to be non-viscous and ideally incompressible. The dynamical critical buckling loads are evaluated by the Budiansky–Roth criterion in three cases: axial compression and lateral pressure with movable and immovable boundary conditions are obtained using the Galerkin method. Moreover, effects of geometrical and material parameters, imperfection and fluid on the nonlinear dynamical buckling behavior of shells are shown in the obtained results.

## 1 Introduction

The problems of structures containing fluid have been attracting vast attention of researchers around the world. Chen et al. [1] investigated the vibration of fluid-filled orthotropic FGM cylindrical shells based on the three-dimensional fundamental equations of anisotropic elasticity. The frequency equation was deduced for an FGM cylindrical shell filled with a compressible, non-viscous fluid medium. The vibration analysis of a functionally graded (FG) rectangular plate partially in contact with a bounded fluid was given by Khorshidi and Bakhsheshy [2]. The fluid velocity potential satisfying fluid boundary conditions was derived, and wet dynamic modal functions of the plate were expanded in terms of finite Fourier series for compatibility requirements along the contacting surface between the plate and the fluid. Sheng and Wang [3] proposed an investigation into the vibration of FGM cylindrical shells with flowing fluid in an elastic medium under mechanical and thermal loads. Based on the first-order shear deformation theory (FSDT) and the fluid velocity potential, the dynamic equation of functionally graded cylindrical shells with flowing fluid was derived. The equations of the eigenvalue problem were obtained by using a modal expansion method. A numerical analysis of stability of a stationary or rotating circular cylindrical shell containing axially flowing and rotating fluid was investigated by Bochkarev and Matveenko [4]. The form of stability loss in stationary and rotating shells under the action of the fluid flow, having both axial and circumferential components, depended on the type of the boundary conditions specified

D. H. Bich

Department of Mathematics, Mechanics and Informatics, Vietnam National University, No. 144 Xuan Thuy Street, Cau Giay District, Hanoi, Vietnam

D. G. Ninh (✉)

School of Mechanical Engineering, Hanoi University of Science and Technology, Hanoi, Vietnam

E-mail: ninh.dinhgia@gmail.com; ninh.dinhgia@hust.edu.vn

Tel.: 84 988 287 789

at their ends. A theoretical and an experimental investigation carried out on a thin-walled hemi-ellipsoidal prolate dome in air and also under external water pressure were given by Ross et al. [5]. The theoretical investigation was carried out using the finite element analysis to model both the structure and the fluid. The ANSYS program used 2 different doubly curved thin-walled shell elements, while the in-house program used a simpler axisymmetric thin-walled shell element. This axisymmetric element allowed a sinusoidal variation of the displacements in the circumferential direction, thus decreasing preparation and computational time. Prado et al. [6] studied the dynamic instability of perfect simply supported orthotropic cylindrical shells with internal flowing fluid and subjected to either a compressive axial static preload plus a harmonic axial load or a harmonic lateral pressure. The fluid was assumed to be non-viscous and incompressible and the flow, isentropic and irrotational. An expansion with eight degrees of freedom, containing the fundamental, companion, gyroscopic, and four axisymmetric modes was used to describe the lateral displacement of the shell. An analytical method to predict nondestructively the elastic critical pressure of a submerged cylindrical shell which is subjected to external hydrostatic pressure was presented in Zhu et al. [7]. The structural–fluid coupling dispersion equation of the system was established considering axial and lateral hydrostatic pressure based on the wave propagation approach.

Furthermore, the sandwich structures have become of great interest in structural applications. The smooth and continuous change in material properties enables sandwiched FGMs to avoid interface problems and unexpected thermal stress concentrations. On the other hand, sandwich structures also have other mentionable properties, especially thermal and sound insulation. Sburlati [8] proposed an analytical solution in the framework of elasticity theory to indicate the elastic bending response of axisymmetric circular sandwich panels with functionally graded material cores and homogeneous face sheets. The elastic solution was obtained using a Plevako representation, which reduced the problem to the search of potential functions satisfying linear fourth-order partial differential equations. Sofiyev et al. [9, 10] studied the parametric instability of a simply supported sandwich cylindrical shell with an FGM core under static and time-dependent periodic axial compressive loads and the influences of shear stresses and rotary inertia on the vibration of FG-coated sandwich cylindrical shells resting on a Pasternak elastic foundation. The static and free vibration behaviors of two types of sandwich plates based on the three-dimensional theory of elasticity were carried out by Alibeigloo and Alizadeh [11]. By using differential equilibrium equations and/or equations of motion as well as constitutive relations, the state-space differential equation was derived. Taibi et al. [12] investigated the deformation behavior of shear deformable FG sandwich plates resting on a Pasternak foundation under thermo-mechanical loads. Xia and Shen [13] investigated the small- and large-amplitude vibration of compressively and thermally post-buckled sandwich plates with FGM face sheets in thermal environment using a higher-order shear deformation plate theory. The formulations were based on a general von Karman-type equation that included a thermal effect, and the equations of motion were solved by an improved perturbation technique. The free vibration of sandwich plates with FGM face sheets in various thermal environments to improve high-order sandwich plate theory was studied by Khalili and Mohammadi [14]. The governing equations of motion in free natural vibration were derived using Hamilton's principle. A new approach was used to reduce the equations of motion and then solved them for both unsymmetric and symmetric sandwich plates. Wang and Shen [15] investigated the nonlinear dynamic response of sandwich plates with FGM face sheets resting on elastic foundations in thermal environments. The material properties of the FGM layers were assumed to be graded in the thickness direction according to the Mori–Tanaka scheme.

The dynamic buckling problems for shell structures are investigated widely. Shariyat [16, 17] presented dynamic buckling of a prestressed, suddenly heated imperfect FGM cylindrical shell and dynamic buckling of a mechanically loaded imperfect FGM cylindrical shell in thermal environment, with temperature-dependent properties; dynamic buckling of imperfect FGM cylindrical shells with integrated surface-bonded sensor and actuator layers subjected to some complex combinations of thermo-electromechanical loads. The general form of Green's strain tensor in curvilinear coordinates and a high-order shell theory were proposed. Furthermore, the nonlinear dynamic buckling of FGM cylindrical shells under time-dependent axial load and radial load using an energy method and the Budiansky–Roth criterion were presented by Huang and Han [18, 19]. Bich et al. [20, 21] studied the nonlinear dynamic buckling of FGM cylindrical shells and shallow spherical shells in thermal environment using the Galerkin procedure and Budiansky–Roth criterion. The dynamic instability of simply supported, functionally graded (FG) truncated conical shells under static and time-dependent periodic axial loads using the Galerkin method was analyzed by Sofiyev and Kuruoglu [22]. The domains of principal instability were determined using Bolotin's method. With the same above structures, Sofiyev [23] investigated the dynamic buckling of truncated conical shells with FGM coatings subjected to a time-dependent axial load in large deformation. The method of solution utilizes the superposition principle and the Galerkin procedure.

Donnell–Karman-type nonlinear differential equations for the truncated conical shell with FGCs are derived and reduced to ordinary differential equations with time-dependent coefficient. The nonlinear dynamic of imperfect FGM thick double shallow shells with piezoelectric actuators on elastic foundations under the combination of electrical, thermal, mechanical and damping loading was given by Duc et al. [24]. Zhang and Li [25] discussed dynamic buckling of FGM truncated conical shells subjected to normal impact loads using the Galerkin procedure and Runge–Kutta integration to solve the nonlinear governing equations numerically.

The toroidal shell segment structures have been applied in mechanical engineering, aerospace engineering, biomechanical engineering, and so forth. In the past, there were some studies about these structures. McElman [26] investigated the eccentrically stiffened shallow shells of double curvature with the static and dynamic behaviors in a NASA technical note. The initial post-buckling behavior of toroidal shell segments under several loading conditions using Koiter’s general theory was studied by Hutchinson [27]. Stein and McElman [28] pointed out the buckling of homogenous and isotropic toroidal shell segments. Recently, Bich et al. [29–33] has investigated the stability buckling of functionally graded toroidal shell segment under mechanical load based on the classical thin shell theory and the smeared stiffeners technique. Ninh and Bich [34] have just studied the nonlinear thermal vibration of eccentrically stiffened ceramic–FGM–metal layer toroidal shell segments surrounded by an elastic foundation.

To the best of the authors’ knowledge, this is the first time that the nonlinear dynamical buckling of imperfect eccentrically stiffened three-layered toroidal shell segments fully filled with fluid is investigated. The dynamical critical buckling loads are evaluated by the Budiansky–Roth criterion in three cases: axial compression and lateral pressure with movable and immovable boundary conditions. Based on the classical shell theory with the nonlinear strain-displacement relation of large deflection, the Galerkin method, Volmir’s assumption and a numerical method using fourth-order Runge–Kutta are implemented for dynamic analysis of shells. The fluid is assumed to be non-viscous and ideally incompressible. Effects of geometrical and material parameters, imperfection and fluid on the nonlinear dynamical buckling behavior of shells are illustrated in the obtained results.

## 2 Formulation of the problem

### 2.1 Three-layered composite (FGM core)

The sandwich toroidal shell segment of thickness  $h$ , length  $L$ , which is formed by rotation of a plane circular arc of radius  $R$  about an axis in the plane of the curve as is shown in Fig. 1. The coordinate system  $(x, y, z)$  is located on the middle surface of the shell,  $x$  and  $y$  are the axial and circumferential directions, respectively, and  $z$  is the normal to the shell surface. The thickness of the shell is defined in a coordinate system  $(y, z)$  in Fig. 2. The inner layer ( $z = h/2$ ) and the outer layer ( $z = -h/2$ ) are isotropic and homogenous with ceramic and metal, respectively. Suppose that the material composition of the shell varies smoothly along the thickness in such a way that the inner surface is ceramic, the outer surface is metal, and the core is FGM.

The thickness of the shell, ceramic rich and metal rich is  $h, h_c, h_m$ , respectively. Thus, the thickness of the FGM core is  $h - h_c - h_m$ . The subscripts  $m$  and  $c$  refer to the metal and ceramic constituents, respectively. Denote  $V_m$  and  $V_c$  as volume—fractions of metal and ceramic phases, respectively, where  $V_m + V_c = 1$ . According to the mentioned law, the volume fraction is expressed as

$$\begin{cases} V_c(z) = 0, & -\frac{h}{2} \leq z \leq -\left(\frac{h}{2} - h_m\right), \\ V_c(z) = \left(\frac{z+h/2-h_m}{h-h_c-h_m}\right)^k, & -\left(\frac{h}{2} - h_m\right) \leq z \leq \left(\frac{h}{2} - h_c\right), \quad k \geq 0, \\ V_c(z) = 1, & \left(\frac{h}{2} - h_c\right) \leq z \leq \frac{h}{2}. \end{cases} \quad (1)$$

According to the mentioned law, the Young modulus of the FGM core shell is expressed in the form

$$\begin{aligned} E(z) &= E_m V_m(z) + E_c V_c(z) = E_m + (E_c - E_m)V_c(z), \\ \rho(z) &= \rho_m V_m(z) + \rho_c V_c(z) = \rho_m + (\rho_c - \rho_m)V_c(z), \end{aligned}$$

and the Poisson ratio  $\nu$  is assumed to be constant.

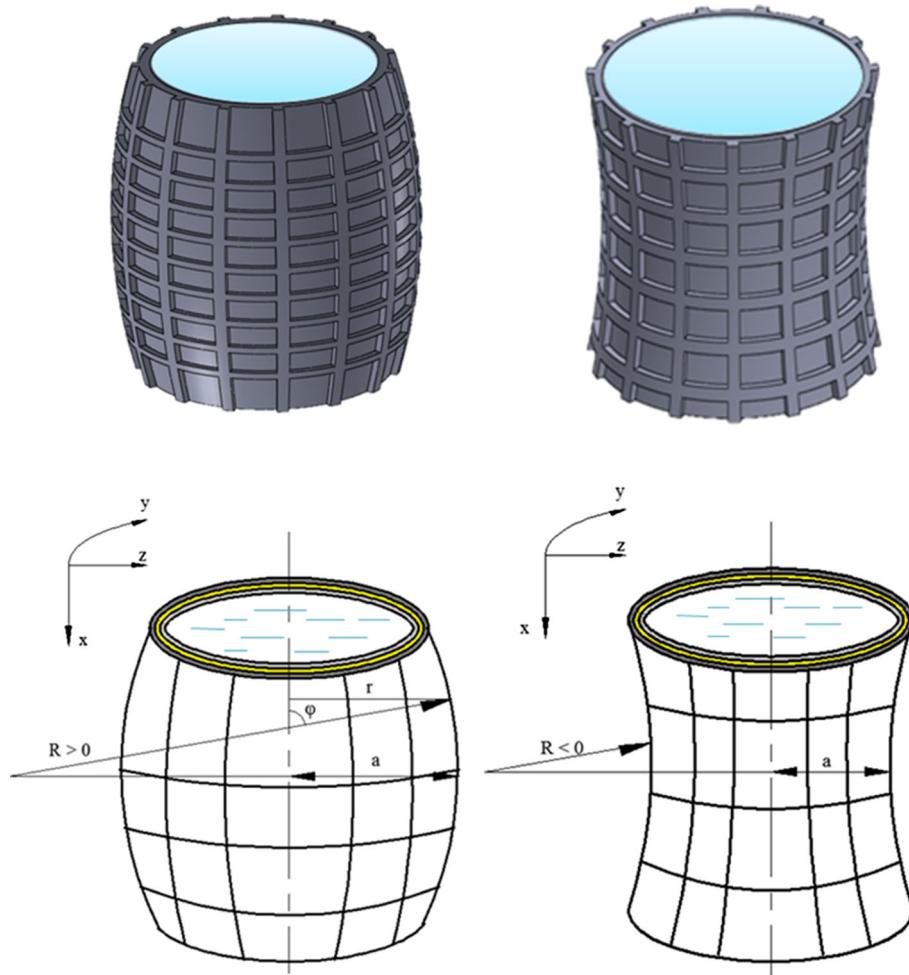


**Fig. 1** Coordinate system of the ES-FGM core toroidal shell segment containing fluid

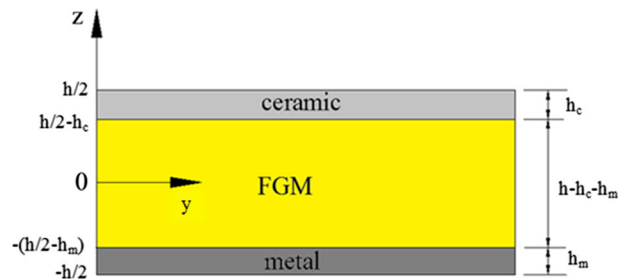


**Fig. 2** Material characteristic of the FGM core

2.2 Constitutive relations and governing equations

Consider a sufficiently shallow toroidal shell segment in the region of the equator of the torus as described in Fig. 1. By the Stein and Mc Elman assumption [28], the angle  $\varphi$  between the axis of revolution and the normal to the shell surface is approximately equal to  $\pi/2$ , thus

$$\sin \varphi \approx 1; \quad \cos \varphi \approx 0; \quad r = a - R(1 - \sin \varphi) \approx a, \\ \text{and } dx = Rd\varphi, \quad dy = ad\theta,$$

where  $a$  is the equator radius and  $\theta$  is the circumferential angle.

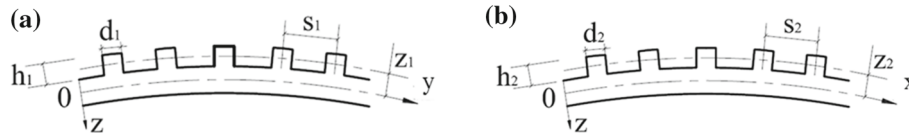


**Fig. 3** Geometry and coordinate system of a stiffened FGM core toroidal shell segment containing fluid **a** stringer stiffeners; **b** ring stiffeners

The radius of arc  $R$  is positive with the convex toroidal shell segment and negative with the concave toroidal shell segment.

Suppose the eccentrically stiffened FGM core toroidal shell segment is reinforced by string and ring stiffeners. In order to provide continuity within the shell and stiffeners and easier manufacture, the homogeneous stiffeners can be used. Because pure ceramic ones are brittle, we used metal stiffeners and put them on the metal side of the shell. With the law indicated in (1), the outer surface is metal, so the external metal stiffeners are put on the outer side of the shell. Figure 3 depicts the geometry and coordinate system of the stiffened FGM core shell.

The von Karman-type nonlinear kinematic relation for the strain component across the shell thickness at a distance  $z$  from the middle surface is of the form [35]

$$\begin{pmatrix} \varepsilon_x \\ \varepsilon_y \\ \gamma_{xy} \end{pmatrix} = \begin{pmatrix} \varepsilon_x^0 \\ \varepsilon_y^0 \\ \gamma_{xy}^0 \end{pmatrix} - z \begin{pmatrix} \chi_x \\ \chi_y \\ 2\chi_{xy} \end{pmatrix}, \quad (2)$$

where  $\varepsilon_x^0$  and  $\varepsilon_y^0$  are normal strains,  $\gamma_{xy}^0$  is the shear strain at the middle surface of the shell,  $\chi_x$  and  $\chi_y$  are the curvatures and  $\chi_{xy}$  is the twist.

According to the classical shell theory, the strains at the middle surface and curvatures are related to the displacement components  $u$ ,  $v$ ,  $w$  in the  $x$ ,  $y$ ,  $z$  coordinate directions as [35]

$$\begin{pmatrix} \varepsilon_x^0 \\ \varepsilon_y^0 \\ \gamma_{xy}^0 \end{pmatrix} = \left\{ \begin{array}{l} \frac{\partial u}{\partial x} - \frac{w}{R} + \frac{1}{2} \left( \frac{\partial w}{\partial x} \right)^2 + \frac{\partial w}{\partial x} \frac{\partial w_o}{\partial x} \\ \frac{\partial v}{\partial y} - \frac{w}{a} + \frac{1}{2} \left( \frac{\partial w}{\partial y} \right)^2 + \frac{\partial w}{\partial y} \frac{\partial w_o}{\partial y} \\ \frac{\partial u}{\partial y} + \frac{\partial v}{\partial x} + \frac{\partial w}{\partial x} \frac{\partial w}{\partial y} + \frac{\partial w}{\partial x} \frac{\partial w_o}{\partial y} + \frac{\partial w}{\partial y} \frac{\partial w_o}{\partial x} \end{array} \right\}; \quad \begin{pmatrix} \chi_x \\ \chi_y \\ \chi_{xy} \end{pmatrix} = \begin{pmatrix} \frac{\partial^2 w}{\partial x^2} \\ \frac{\partial^2 w}{\partial y^2} \\ \frac{\partial^2 w}{\partial x \partial y} \end{pmatrix}, \quad (3)$$

where  $w_o(x, y)$  is a known function representing initial imperfection of the shell.

From Eq. (3), the strains must be satisfied in the deformation compatibility equation

$$\frac{\partial^2 \varepsilon_x^0}{\partial y^2} + \frac{\partial^2 \varepsilon_y^0}{\partial x^2} - \frac{\partial^2 \gamma_{xy}^0}{\partial x \partial y} = -\frac{\partial^2 w}{R \partial y^2} - \frac{\partial^2 w}{a \partial x^2} + \left( \frac{\partial^2 w}{\partial x \partial y} + \frac{\partial^2 w_o}{\partial x \partial y} \right)^2 - \left( \frac{\partial^2 w}{\partial x^2} + \frac{\partial^2 w_o}{\partial x^2} \right) \left( \frac{\partial^2 w}{\partial y^2} + \frac{\partial^2 w_o}{\partial y^2} \right). \quad (4)$$

Hooke's law for the toroidal shell segment is defined as

$$\begin{aligned} \sigma_x^{sh} &= \frac{E(z)}{1-\nu^2} (\varepsilon_x + \nu \varepsilon_y), \\ \sigma_y^{sh} &= \frac{E(z)}{1-\nu^2} (\varepsilon_y + \nu \varepsilon_x), \\ \sigma_{xy}^{sh} &= \frac{E(z)}{2(1+\nu)} \gamma_{xy}, \end{aligned} \quad (5)$$

and for the metal stiffeners

$$\sigma_x^{st} = E_m \varepsilon_x; \quad \sigma_y^{st} = E_m \varepsilon_y.$$

By integrating the stress–strain equations and their moments through the thickness of the shell and using the smeared stiffeners technique, the expressions for force and moment resultants of a FGM core toroidal shell segment can be obtained as [33,35]:

$$\begin{aligned}
N_x &= \left( A_{11} + \frac{E_m A_1}{s_1} \right) \varepsilon_x^0 + A_{12} \varepsilon_y^0 - (B_{11} + C_1) \chi_x - B_{12} \chi_y, \\
N_y &= A_{12} \varepsilon_x^0 + \left( A_{22} + \frac{E_m A_2}{s_2} \right) \varepsilon_y^0 - B_{12} \chi_x - (B_{22} + C_2) \chi_y, \\
N_{xy} &= A_{66} \gamma_{xy}^0 - 2B_{66} \chi_{xy},
\end{aligned} \tag{6}$$

$$\begin{aligned}
M_x &= (B_{11} + C_1) \varepsilon_x^0 + B_{12} \varepsilon_y^0 - \left( D_{11} + \frac{E_m I_1}{s_1} \right) \chi_x - D_{12} \chi_y, \\
M_y &= B_{12} \varepsilon_x^0 + (B_{22} + C_2) \varepsilon_y^0 - D_{12} \chi_x - \left( D_{22} + \frac{E_m I_2}{s_2} \right) \chi_y, \\
M_{xy} &= B_{66} \gamma_{xy}^0 - 2D_{66} \chi_{xy},
\end{aligned} \tag{7}$$

where  $A_{ij}$ ,  $B_{ij}$ ,  $D_{ij}$  ( $i, j = 1, 2, 6$ ) are extensional, coupling and bending stiffnesses of the shell without stiffeners:

$$\begin{aligned}
A_{11} = A_{22} &= \frac{E_1}{1 - \nu^2}, \quad A_{12} = \frac{E_1 \nu}{1 - \nu^2}, \quad A_{66} = \frac{E_1}{2(1 + \nu)}, \\
B_{11} = B_{22} &= \frac{E_2}{1 - \nu^2}, \quad B_{12} = \frac{E_2 \nu}{1 - \nu^2}, \quad B_{66} = \frac{E_2}{2(1 + \nu)}, \\
D_{11} = D_{22} &= \frac{E_3}{1 - \nu^2}, \quad D_{12} = \frac{E_3 \nu}{1 - \nu^2}, \quad D_{66} = \frac{E_3}{2(1 + \nu)},
\end{aligned} \tag{8}$$

where

$$\begin{aligned}
E_1 &= \int_{-h/2}^{h/2} E(z) dz = E_1 = E_m h + E_{cm} h_c + \frac{E_{cm}(h - h_c - h_m)}{k + 1}, \\
E_2 &= \int_{-h/2}^{h/2} E(z) z dz = E_2 = \frac{E_{cm} h_c h}{2} - \frac{E_{cm} h_c^2}{2} + \frac{E_{cm}}{k + 1} \left( \frac{h}{2} - h_c \right) (h - h_c - h_m) \\
&\quad - \frac{E_{cm}}{(k + 1)(k + 2)} (h - h_c - h_m)^2, \\
E_3 &= \int_{-h/2}^{h/2} E(z) z^2 dz = E_3 = \frac{E_{cm}}{k + 1} \left( \frac{h}{2} - h_c \right)^2 (h - h_c - h_m) - \frac{2E_{cm}}{(k + 1)(k + 2)} \left( \frac{h}{2} - h_c \right) (h - h_c - h_m)^2 \\
&\quad + \frac{2E_{cm}}{(k + 1)(k + 2)(k + 3)} (h - h_c - h_m)^3 + \frac{E_c h_c^3}{3} \\
&\quad + \frac{E_c h h_c}{2} \left( \frac{h}{2} - h_c \right) + \frac{E_m}{3} \left[ h_m^3 + \frac{3h h_m}{2} \left( \frac{h}{2} - h_m \right) \right] + \frac{E_m}{3} \left[ (h - h_c - h_m)^3 - 3 \left( \frac{h}{2} - h_m \right) \right. \\
&\quad \left. \times \left( \frac{h}{2} - h_c \right) (h - h_c - h_m) \right],
\end{aligned}$$

in which  $E_{cm} = E_c - E_m$ , and

$$\begin{aligned}
C_1 &= -\frac{E_m A_1 z_1}{s_1}, \quad C_2 = -\frac{E_m A_2 z_2}{s_2}, \\
A_1 &= h_1 d_1, \quad A_2 = h_2 d_2, \\
I_1 &= \frac{d_1 h_1^3}{12} + A_1 z_1^2, \quad I_2 = \frac{d_2 h_2^3}{12} + A_2 z_2^2.
\end{aligned}$$

The spacings of the stringer and ring stiffeners are denoted by  $s_1$  and  $s_2$ , respectively. The quantities  $A_1, A_2$  are the cross-sectional areas of the stiffeners, and  $I_1, I_2, z_1, z_2$  are the second moments of cross-sectional areas and eccentricities of the stiffeners with respect to the middle surface of the shell, respectively.

The reverse relations are obtained from Eq. (6) as

$$\begin{aligned}\varepsilon_x^0 &= A_{22}^* N_x - A_{12}^* N_y + B_{11}^* \chi_x + B_{12}^* \chi_y, \\ \varepsilon_y^0 &= A_{11}^* N_y - A_{12}^* N_x + B_{21}^* \chi_x + B_{22}^* \chi_y, \\ \gamma_{xy}^0 &= A_{66}^* N_{xy} + 2B_{66}^* \chi_{xy}.\end{aligned}\quad (9)$$

Substituting Eq. (9) into Eq. (7) yields

$$\begin{aligned}M_x &= B_{11}^* N_x + B_{21}^* N_y - D_{11}^* \chi_x - D_{12}^* \chi_y, \\ M_y &= B_{12}^* N_x + B_{22}^* N_y - D_{21}^* \chi_x - D_{22}^* \chi_y, \\ M_{xy} &= B_{66}^* N_{xy} - 2D_{66}^* \chi_{xy},\end{aligned}\quad (10)$$

where

$$\begin{aligned}A_{11}^* &= \frac{1}{\Delta} \left( A_{11} + \frac{E_m A_1}{s_1} \right), \quad A_{22}^* = \frac{1}{\Delta} \left( A_{22} + \frac{E_m A_2}{s_2} \right), \quad A_{12}^* = \frac{A_{12}}{\Delta}, \quad A_{66}^* = \frac{1}{A_{66}}, \\ \Delta &= \left( A_{11} + \frac{E_m A_1}{s_1} \right) \cdot \left( A_{22} + \frac{E_m A_2}{s_2} \right) - A_{12}^2, \\ B_{11}^* &= A_{22}^* (B_{11} + C_1) - A_{12}^* B_{12}, \quad B_{22}^* = A_{11}^* (B_{22} + C_2) - A_{12}^* B_{12}, \\ B_{12}^* &= A_{22}^* B_{12} - A_{12}^* (B_{22} + C_2), \quad B_{21}^* = A_{11}^* B_{12} - A_{12}^* (B_{11} + C_1), \quad B_{66}^* = \frac{B_{66}}{A_{66}}, \\ D_{11}^* &= D_{11} + \frac{E_m I_1}{s_1} - (B_{11} + C_1) B_{11}^* - B_{12} B_{21}^*, \\ D_{22}^* &= D_{22} + \frac{E_m I_2}{s_2} - B_{12} B_{21}^* - (B_{22} + C_2) B_{22}^*, \\ D_{12}^* &= D_{12} - (B_{11} + C_1) B_{12}^* - B_{12} B_{22}^*, \\ D_{21}^* &= D_{12} - B_{12} B_{11}^* - (B_{22} + C_2) B_{21}^*, \\ D_{66}^* &= D_{66} - B_{66} B_{66}^*.\end{aligned}$$

The nonlinear equilibrium equations of a toroidal shell segment filled inside by an incompressible fluid under a lateral pressure  $q$  and an axial compression  $p$  based on the classical shell theory are given by [35]:

$$\begin{aligned}\frac{\partial N_x}{\partial x} + \frac{\partial N_{xy}}{\partial y} &= \rho_1 \frac{\partial^2 u}{\partial t^2}, \\ \frac{\partial N_{xy}}{\partial x} + \frac{\partial N_y}{\partial y} &= \rho_1 \frac{\partial^2 v}{\partial t^2}, \\ \frac{\partial^2 M_x}{\partial x^2} + 2 \frac{\partial^2 M_{xy}}{\partial x \partial y} + \frac{\partial^2 M_y}{\partial y^2} + N_x \left( \frac{\partial^2 w}{\partial x^2} + \frac{\partial^2 w_o}{\partial x^2} \right) + 2N_{xy} \left( \frac{\partial^2 w}{\partial x \partial y} + \frac{\partial^2 w_o}{\partial x \partial y} \right) \\ + N_y \left( \frac{\partial^2 w}{\partial y^2} + \frac{\partial^2 w_o}{\partial y^2} \right) + \frac{N_x}{R} + \frac{N_y}{a} + q &= \rho_1 \frac{\partial^2 w}{\partial t^2} + 2 \rho_1 \varepsilon \frac{\partial w}{\partial t} - p_L,\end{aligned}\quad (11)$$

where  $\varepsilon$  is the damping coefficient,  $p_L$  is the dynamic fluid pressure acting on the shell and

$$\rho_1 = \rho_m h + \rho_{cm} h_c + \frac{\rho_{cm} (h - h_c - h_m)}{k + 1} + \rho_m \left( \frac{A_1}{s_1} + \frac{A_2}{s_2} \right).\quad (12)$$



### 2.3 The dynamic pressure of fluid acting on the shell

The dynamic pressure of fluid acting on shell is expressed as follows:

$$p_L = -\rho_L \frac{\partial \varphi_L}{\partial t}, \quad (13)$$

where  $\rho_L$  is the mass density of the fluid.

According to the Stein and McElman assumption [28], for a shallow toroidal shell segment the equation of the fluid velocity potential can be written approximately in the cylindrical coordinate system  $(x, \theta, r)$  as

$$\frac{\partial^2 \varphi_L}{\partial r^2} + \frac{1}{r} \frac{\partial \varphi_L}{\partial r} + \frac{1}{r^2} \frac{\partial \varphi_L}{\partial \theta^2} + \frac{\partial^2 \varphi_L}{\partial x^2} = 0 \quad (14)$$

with the boundary condition

$$\frac{\partial \varphi_L}{\partial r} = -\frac{\partial w}{\partial t} \quad \text{at } r = a. \quad (15)$$

$\varphi_L$  has to be finite when  $r = 0$  and at  $x = 0$ ;  $L$  it depends on the boundary condition of the shell. Supposing the shell is simply supported at  $x = 0$  and  $x = L$ , the vibration shape function of shell can be chosen as

$$w = \sum \sum f_{mn}(t) \sin \frac{m\pi x}{L} \sin n\theta. \quad (16)$$

Then, the solution of Eq. (14) can be expressed as

$$\varphi_L = \sum \sum A_{mn}(t) I_n \left( \frac{m\pi r}{L} \right) \sin \frac{m\pi x}{L} \sin n\theta, \quad (17)$$

in which  $I_n$  is the Bessel function of the first kind of order  $n$ .

Certainly substitution of Eq. (17) into the left side of Eq. (14) leads to the identity. Satisfying the boundary condition (15) with the use of Eqs. (16), (17), we obtain

$$A_{mn}(t) = \frac{-L}{m\pi I_n' \left( \frac{m\pi a}{L} \right)} \frac{df_{mn}}{dt}.$$

Putting the just obtained result into Eq. (17) and comparing with Eq. (16) yields

$$\varphi_L = -\frac{a I_n(\lambda_m)}{\lambda_m I_n'(\lambda_m)} \frac{\partial w}{\partial t}, \quad (\lambda_m = \frac{m\pi a}{L}). \quad (18)$$

Substituting Eq. (18) into the left side of Eq. (13), the expression of the dynamic fluid pressure acting on the shell is obtained:

$$p_L = -\rho_L \frac{\partial \varphi_L}{\partial t} = \rho_L \frac{a I_n(\lambda_m)}{\lambda_m I_n'(\lambda_m)} \frac{\partial^2 w}{\partial t^2} = m_L \frac{\partial^2 w}{\partial t^2}, \quad (19)$$

in which  $m_L = \frac{\rho_L a I_n(\lambda_m)}{\lambda_m I_n'(\lambda_m)}$  ( $m_L$  is the mass of fluid corresponding to the vibration of the shell)



### 3 Nonlinear dynamic buckling analysis of fully fluid-filled imperfect FGM core toroidal shell segment

Putting the expression of dynamic fluid pressure (19) into Eq. (11) and using Volmir’s assumption [36]  $\rho_1(\partial^2 u/\partial t^2) \rightarrow 0$ ,  $\rho_1(\partial^2 v/\partial t^2) \rightarrow 0$  because of  $u \ll w$ ,  $v \ll w$ , we can rewrite the system of the equations of motion (11) as follows:

$$\begin{aligned} \frac{\partial N_x}{\partial x} + \frac{\partial N_{xy}}{\partial y} &= 0, \\ \frac{\partial N_{xy}}{\partial x} + \frac{\partial N_y}{\partial y} &= 0, \\ \frac{\partial^2 M_x}{\partial x^2} + 2\frac{\partial^2 M_{xy}}{\partial x \partial y} + \frac{\partial^2 M_y}{\partial y^2} + N_x \left( \frac{\partial^2 w}{\partial x^2} + \frac{\partial^2 w_o}{\partial x^2} \right) + 2N_{xy} \left( \frac{\partial^2 w}{\partial x \partial y} + \frac{\partial^2 w_o}{\partial x \partial y} \right) \\ + N_y \left( \frac{\partial^2 w}{\partial y^2} + \frac{\partial^2 w_o}{\partial y^2} \right) + \frac{N_x}{R} + \frac{N_y}{a} + q &= (\rho_1 + m_L) \frac{\partial^2 w}{\partial t^2} + 2\rho_1 \varepsilon \frac{\partial w}{\partial t}. \end{aligned} \tag{20}$$

Two first equations of Eq. (20) are satisfied identically by introducing the stress function as:

$$N_x = \frac{\partial^2 F}{\partial y^2}, \quad N_y = \frac{\partial^2 F}{\partial x^2}, \quad N_{xy} = -\frac{\partial^2 F}{\partial x \partial y}. \tag{21}$$

Substituting Eq. (9) into deformation compatibility Eq. (4) and substituting Eq. (10) into the third equation of motion (20), taking into account expressions (3) and (21), yields a system of equations:

$$\begin{aligned} A_{11}^* \frac{\partial^4 F}{\partial x^4} + (A_{66}^* - 2A_{12}^*) \frac{\partial^4 F}{\partial x^2 \partial y^2} + A_{22}^* \frac{\partial^4 F}{\partial y^4} + B_{21}^* \frac{\partial^4 w}{\partial x^4} + (B_{11}^* + B_{22}^* - 2B_{66}^*) \frac{\partial^4 w}{\partial x^2 \partial y^2} \\ + B_{12}^* \frac{\partial^4 w}{\partial y^4} + \frac{1}{R} \frac{\partial^2 w}{\partial y^2} + \frac{1}{a} \frac{\partial^2 w}{\partial x^2} + \left( \frac{\partial^2 w}{\partial x \partial y} \right)^2 + \frac{\partial^2 w}{\partial x^2} \frac{\partial^2 w}{\partial y^2} \\ - 2 \frac{\partial^2 w}{\partial x \partial y} \frac{\partial^2 w_o}{\partial x \partial y} + \frac{\partial^2 w}{\partial x^2} \frac{\partial^2 w_o}{\partial y^2} + \frac{\partial^2 w}{\partial y^2} \frac{\partial^2 w_o}{\partial x^2} = 0, \tag{22} \\ (\rho_1 + m_L) \frac{\partial^2 w}{\partial t^2} + 2\rho_1 \varepsilon \frac{\partial w}{\partial t} + D_{11}^* \frac{\partial^4 w}{\partial x^4} + (D_{12}^* + D_{21}^* + 4D_{66}^*) \frac{\partial^4 w}{\partial x^2 \partial y^2} \\ + D_{22}^* \frac{\partial^4 w}{\partial y^4} - B_{21}^* \frac{\partial^4 F}{\partial x^4} - (B_{11}^* + B_{22}^* - 2B_{66}^*) \frac{\partial^4 F}{\partial x^2 \partial y^2} \\ - B_{12}^* \frac{\partial^4 F}{\partial y^4} - \frac{1}{R} \frac{\partial^2 F}{\partial y^2} - \frac{1}{a} \frac{\partial^2 F}{\partial x^2} - \frac{\partial^2 F}{\partial y^2} \left( \frac{\partial^2 w}{\partial x^2} + \frac{\partial^2 w_o}{\partial x^2} \right) + 2 \frac{\partial^2 F}{\partial x \partial y} \left( \frac{\partial^2 w}{\partial x \partial y} + \frac{\partial^2 w_o}{\partial x \partial y} \right) \\ - \frac{\partial^2 F}{\partial x^2} \left( \frac{\partial^2 w}{\partial y^2} + \frac{\partial^2 w_o}{\partial y^2} \right) = q. \end{aligned} \tag{23}$$

Equations (22) and (23) are the nonlinear governing equations used to investigate the nonlinear dynamic buckling of fully fluid-filled imperfect eccentrically stiffened FGM core toroidal shell segments.

Depending on the type of loading and the in-plane behavior at the edge, three cases of boundary condition can be considered.

**Case 1:** The shell is simply supported and subjected to axial compressive load  $N_{01} = -p_o h$ , where  $p_o$  is the average axial stress on the shell edges. Then, the associated boundary conditions are

$$w = 0, M_x = 0, N_x = N_{01} = -p_o h, N_{xy} = 0 \quad \text{at } x = 0; L. \tag{24}$$

**Case 2:** The shell is simply supported and freely movable in the axial direction. The shell is acted on by lateral pressure uniformly distributed on the outer surface of shell. The boundary condition in this case is the following:

$$w = 0, M_x = 0, N_x = 0, N_{xy} = 0 \quad \text{at } x = 0; L. \tag{25}$$

**Case 3:** The shell is simply supported with immovable edges and subjected to lateral pressure on the outer surface of the shell. The boundary conditions for this case can be expressed as

$$u = 0, w = 0, M_x = 0, N_x = N_{01}, N_{xy} = 0 \quad \text{at } x = 0; L, \quad (26)$$

where  $N_{01}$  is the fictitious compressive edge load rendering the edge immovable.

With the consideration of compatibility of shell and fluid on the interacted shell surface, the deflection and the imperfection of the shell can be expressed by:

$$\begin{aligned} w &= f(t) \sin \gamma_m x \sin \beta_n y, \\ w_o &= f_o \sin \gamma_m x \sin \beta_n y, \end{aligned} \quad (27)$$

where  $\gamma_m = \frac{m\pi}{L}$ ;  $\beta_n = \frac{n}{2a}$  and  $m, n$  are the half wave numbers along the  $x$ -axis and wave numbers along the  $y$ -axis, respectively.  $f_o$  is constant,  $f_o$  can be put as:  $f_o = \mu h$  ( $0 \leq \mu < 1$ ),  $h$  is the thickness of shell.

Substituting Eq. (27) into the left side of Eq. (22), the solution for the stress function  $F$  of this equation can be expressed as:

$$F = F_1 \cos 2\gamma_m x + F_2 \cos 2\beta_n y - F_3 \sin \gamma_m x \sin \beta_n y + N_{01} \frac{y^2}{2}, \quad (28)$$

in which

$$\begin{aligned} F_1 &= F_1^* f(f + 2f_o), \\ F_2 &= F_2^* f(f + 2f_o), \\ F_3 &= F_3^* f, \\ F_1^* &= \frac{\beta_n^2}{8\gamma_m^2 A_{11}^*}, \\ F_2^* &= \frac{\gamma_m^2}{8\beta_n^2 A_{22}^*}, \\ F_3^* &= \frac{B_{21}^* \gamma_m^4 + 2(B_{11}^* + B_{22}^* - 2B_{66}^*) \gamma_m^2 \beta_n^2 + 16B_{12}^* \beta_n^4 - 4\beta_n^2/R - \gamma_m^2/a}{A_{11}^* \gamma_m^4 + 2(A_{66}^* - 2A_{12}^*) \gamma_m^2 \beta_n^2 + 16A_{22}^* \beta_n^4}. \end{aligned}$$

Substituting Eq. (27) and (28) into the equations of motion (23) and then applying Galerkin's procedure in the range  $0 \leq x \leq L$ ;  $0 \leq y \leq 2\pi a$ , we obtain the following equation:

$$\begin{aligned} (\rho_1 + m_L) \frac{\partial^2 f}{\partial t^2} + 2\rho_1 \varepsilon \frac{\partial f}{\partial t} + H_1 f^3 \\ + H_2 f^2 + H_3 f + N_{o1} \gamma_m^2 f + N_{o1} \gamma_m^2 f_o - N_{o1} \frac{\delta_1 \delta_2}{R \gamma_m \beta_n} \frac{2}{L \pi a} - q \frac{\delta_1 \delta_2}{\gamma_m \beta_n} \frac{2}{L \pi a} = 0, \end{aligned} \quad (29)$$

in which

$$\begin{aligned} H_1 &= 2\gamma_m^2 \beta_n^2 (F_1^* + F_2^*), \\ H_2 &= 6\gamma_m^2 \beta_n^2 f_o (F_1^* + F_2^*) + \frac{2\delta_1 \delta_2}{3\gamma_m \beta_n L \pi a} \left( 16F_1^* \gamma_m^4 B_{21}^* + 16F_2^* \beta_m^4 B_{12}^* - \frac{4\gamma_m^2 F_1^*}{a} - \frac{4\beta_m^2 F_2^*}{R} \right) \\ &\quad + \frac{20}{9} \frac{\gamma_m \beta_n \delta_1 \delta_2 F_3^*}{L \pi a}, \\ H_3 &= D_{11}^* \gamma_m^4 + (D_{12}^* + D_{21}^* + 4D_{66}^*) \gamma_m^2 \beta_n^2 + D_{22}^* \beta_n^4 \\ &\quad + B_{21}^* \gamma_m^4 F_3^* + (B_{11}^* + B_{22}^* - 2B_{66}^*) \gamma_m^2 \beta_n^2 F_3^* + B_{12}^* \beta_m^4 F_3^* - \frac{\beta_n^2}{R} F_3^* - \frac{\gamma_m^2}{a} F_3^* + 4\gamma_m^2 \beta_n^2 f_o^2 (F_1^* + F_2^*) \\ &\quad + \frac{4\delta_1 \delta_2 f_o}{3\gamma_m \beta_n L \pi a} \left( 16F_1^* \gamma_m^4 B_{21}^* + 16F_2^* \beta_m^4 B_{12}^* - \frac{4\gamma_m^2 F_1^*}{a} - \frac{4\beta_m^2 F_2^*}{R} \right) + \frac{20}{9} \frac{\gamma_m \beta_n \delta_1 \delta_2 f_o F_3^*}{L \pi a}, \end{aligned}$$

$$\delta_1 = (-1)^m - 1 \quad \text{and} \quad \delta_2 = (-1)^n - 1.$$

Equation (29) is the equation of motion to investigate the nonlinear dynamical buckling of fully fluid-filled imperfect three-layered toroidal shell segment.

Using the fourth-order Runge–Kutta method into Eq. (29) combined with the initial conditions, the non-linear responses of fluid full-filled imperfect three-layered toroidal shell segments can be investigated.

The nonlinear dynamic buckling of the mentioned shells can be performed in three cases:

**Case 1:** the shell under compression varying as linear function of time, i.e.,  $q = 0$ ,  $N_{01} = -p_o h$  with  $p_o = c_1 t$  ( $c_1$  is a loading speed).

**Case 2:** the shell with movable edge under lateral pressure varying as linear function of time, i.e.,  $N_{01} = 0$ ,  $q = c_2 t$  ( $c_2$  is a loading speed).

**Case 3:** the shell with immovable edge under lateral pressure varying as linear function of time. In this case,  $q = c_2 t$ ,  $N_{01} \neq 0$ , where  $N_{01}$  now plays a role as the fictitious compressive edge load rendering the edge immovable.

The condition expressing the immovability on the boundary edges, i.e.,  $u = 0$  at  $x = 0$ ;  $L$  is fulfilled in the average sense as

$$\int_0^L \int_0^{2\pi a} \frac{\partial u}{\partial x} dx dy = \int_0^L \int_0^{2\pi a} \left[ \varepsilon_x^0 + \frac{w}{R} - \frac{1}{2} \left( \frac{\partial w}{\partial x} \right)^2 - \frac{\partial w}{\partial x} \frac{\partial w_o}{\partial x} \right] dx dy = 0. \tag{30}$$

Using Eqs. (9), (21), (27) and (28), the integral becomes:

$$\frac{A_{22}^* \beta_n F_3^* \delta_1 \delta_2}{\gamma_m} f + 2N_{01} A_{22}^* L \pi a - \frac{A_{12}^* \gamma_m F_3^* \delta_1 \delta_2}{\beta_n} f - \frac{B_{11}^* \gamma_m \delta_1 \delta_2}{\beta_n} f - \frac{B_{12}^* \beta_n \delta_1 \delta_2}{\gamma_m} f + \frac{\delta_1 \delta_2}{R \gamma_m \beta_n} f - \frac{\gamma_m^2 L \pi a}{4} f^2 - \frac{\gamma_m^2 L \pi a}{2} f_o f = 0$$

$$N_{01} = -\frac{\gamma_m^2}{8A_{22}^*} f^2 - \Phi f, \tag{31}$$

where

$$\Phi = -\left[ -\frac{A_{22}^* \beta_n F_3^* \delta_1 \delta_2}{\gamma_m} + \frac{A_{12}^* \gamma_m F_3^* \delta_1 \delta_2}{\beta_n} + \frac{B_{11}^* \gamma_m \delta_1 \delta_2}{\beta_n} + \frac{B_{12}^* \beta_n \delta_1 \delta_2}{\gamma_m} - \frac{\delta_1 \delta_2}{R \gamma_m \beta_n} + \frac{\gamma_m^2 L \pi a}{2} f_o \right] \frac{1}{2A_{22}^* L \pi a}.$$

Substituting Eq. (31) into the equation of motion (29) yields

$$(\rho_1 + m_L) \frac{\partial^2 f}{\partial t^2} + 2\rho_1 \varepsilon \frac{\partial f}{\partial t} + H_1^* f^3 + H_2^* f^2 + H_3^* f - q \frac{\delta_1 \delta_2}{\gamma_m \beta_n} \frac{2}{L \pi a} = 0, \tag{32}$$

in which

$$\begin{aligned} H_1^* &= 2\gamma_m^2 \beta_n^2 (F_1^* + F_2^*) + \gamma_m^4 / (8A_{22}^*), \\ H_2^* &= 6\gamma_m^2 \beta_n^2 f_o (F_1^* + F_2^*) + \frac{2\delta_1 \delta_2}{3\gamma_m \beta_n L \pi a} \left( 16F_1^* \gamma_m^4 B_{21}^* + 16F_2^* \beta_m^4 B_{12}^* - \frac{4\gamma_m^2 F_1^*}{a} - \frac{4\beta_m^2 F_2^*}{R} \right) \\ &\quad - \frac{20}{9} \frac{\gamma_m \beta_n \delta_1 \delta_2 F_3^*}{L \pi a} - \Phi \gamma_m^2 - \gamma_m^4 f_o / (8A_{22}^*) + \frac{\delta_1 \delta_2 \gamma_m}{4R \beta_n L \pi a A_{22}^*}, \\ H_3^* &= D_{11}^* \gamma_m^4 + (D_{12}^* + D_{21}^* + 4D_{66}^*) \gamma_m^2 \beta_n^2 + D_{22}^* \beta_n^4 \\ &\quad + B_{21}^* \gamma_m^4 F_3^* + (B_{11}^* + B_{22}^* - 2B_{66}^*) \gamma_m^2 \beta_n^2 F_3^* + B_{12}^* \beta_n^4 F_3^* - \frac{\beta_n^2}{R} F_3^* - \frac{\gamma_m^2}{a} F_3^* \\ &\quad + 4\gamma_m^2 \beta_n^2 f_o^2 (F_1^* + F_2^*) + \frac{4\delta_1 \delta_2 f_o}{3\gamma_m \beta_n L \pi a} \left( 16F_1^* \gamma_m^4 B_{21}^* + 16F_2^* \beta_m^4 B_{12}^* - \frac{4\gamma_m^2 F_1^*}{a} - \frac{4\beta_m^2 F_2^*}{R} \right) \\ &\quad - \frac{20}{9} \frac{\gamma_m \beta_n \delta_1 \delta_2 f_o F_3^*}{L \pi a} - \Phi \gamma_m^2 f_o + \frac{2\delta_1 \delta_2}{R \gamma_m \beta_n L \pi a} \Phi. \end{aligned}$$

**Table 1** Comparisons of dynamic critical stress (MPa) of perfect un-stiffened FGM cylindrical shells under linear-time compression

| Parameters                          | Present        | Huang and Han [18] |
|-------------------------------------|----------------|--------------------|
| $a/h = 500, L/a = 2, k = 0.5$       |                |                    |
| $c = 100$ MPa/s                     | 181.76 (2, 11) | 181.67 (2, 11)     |
| $c = 50$ MPa/s                      | 180.45 (2, 11) | 179.37 (2, 11)     |
| $c = 10$ MPa/s                      | 178.02 (1, 8)  | 177.97 (1, 8)      |
| $a/h = 500, L/a = 2, c = 100$ MPa/s |                |                    |
| $k = 0.2$                           | 195.19 (2, 11) | 194.94 (2, 11)     |
| $k = 1.0$                           | 170.25 (2, 11) | 169.94 (2, 11)     |
| $k = 5.0$                           | 150.46 (2, 11) | 150.25 (2, 11)     |
| $L/a = 2, k = 0.2, c = 100$ MPa/s   |                |                    |
| $a/h = 800$                         | 125.37 (2, 11) | 124.91 (2, 12)     |
| $a/h = 600$                         | 162.43 (3, 14) | 162.25 (3, 14)     |
| $a/h = 400$                         | 239.77 (5, 15) | 239.18 (5, 15)     |

By solving Eq. (29) for each case 1 and case 2, respectively, and Eq. (32) for case 3, the dynamical critical time  $t_{cr}$  can be obtained according to Budiansky–Roth criterion [37].

The criterion is based on that, for large value of loading speed, the amplitude–time curve of obtained displacement response increases sharply depending on time, and this curve obtains a maximum by passing from the slope point and at the corresponding time  $t = t_{cr}$  the stability loss occurs. Here  $t = t_{cr}$  is called critical time and the load corresponding to this critical time is called dynamic critical buckling load  $p_{cr} = c_1 t_{cr}$  (in case 1) or  $q_{cr} = c_2 t_{cr}$  (in case 2 or 3), respectively.

## 4 Results and discussion

### 4.1 Validations

To the best of the authors' knowledge, there are no any publications about dynamic buckling imperfect three-layered toroidal shell segments containing full-filled fluid. Thus, the results in this paper are compared with an FGM cylindrical shell (i.e., a toroidal shell segment with  $R \rightarrow \infty$ ).

The results of dynamic buckling of perfect un-stiffened FGM cylindrical shells subjected to linear-time compression without containing fluid are illustrated in Table 1. The results were also compared with these of Huang and Han [18] using the energy method and classical shell theory. It is observed in Table 1 that good agreement is obtained in this comparison.

### 4.2 The results of toroidal shell segments

In the next sections, the paper will take into account dynamical buckling load of imperfect three-layered toroidal shell segments containing fluid under mechanical loads, and effects of geometrical parameters, imperfections, and fluid are considered. The materials consist of aluminum and alumina with  $E_m = 70 \times 10^9$  N/m<sup>2</sup>;  $\rho_m = 2702$  kg/m<sup>3</sup>;  $E_c = 380 \times 10^9$  N/m<sup>2</sup>;  $\rho_c = 3800$  kg/m<sup>3</sup>, and Poisson's ratio is chosen to be 0.3. The density of the fluid is chosen as  $\rho_L = 1000$  kg/m<sup>3</sup>. The parameters  $n_1 = 50$  and  $n_2 = 50$  are the number of stringer and ring stiffeners, respectively.

#### 4.2.1 Case 1: Movable case with axial compression load

**4.2.1.1 Effects of  $R/h$  ratio** Figures 4 and 5 describe the effects of the ratio  $R/h$  on dynamical buckling loads of imperfect stiffened three-layered convex and concave shell, respectively, subjected axial compression load without fluid and fully-filled with fluid. As can be seen, for convex shells the dynamical critical buckling load of fully fluid-filled shell is greater about three times than that of the shell without fluid, while for concave shells this is about four times greater. This means that when the shells contains fluid, the dynamic critical buckling will increase due to the "added mass effect." Furthermore, the amplitudes of deflection of fully-filled shells are higher than these of shells without fluid about 2.3 times and 2.7 times for convex shell and concave shell, respectively.

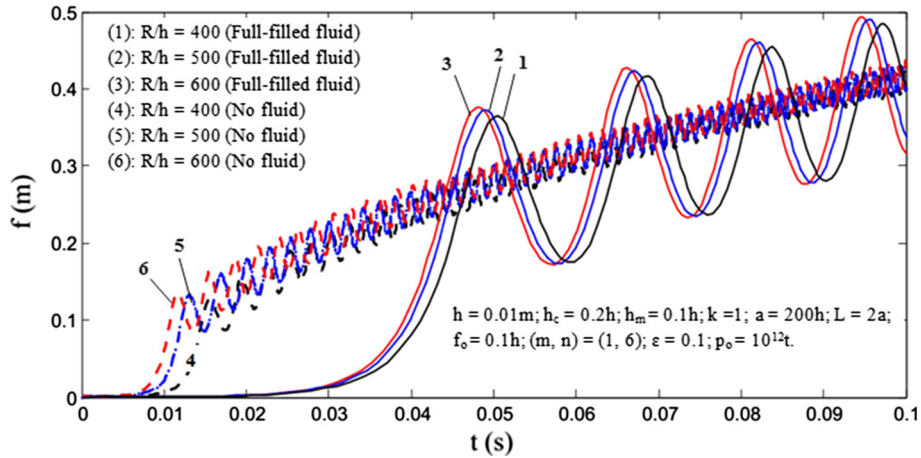


**Fig. 4** Effect of  $R/h$  ratio on dynamical buckling load of imperfect stiffened three-layered convex shells containing full-filled fluid and no fluid under axial compression load

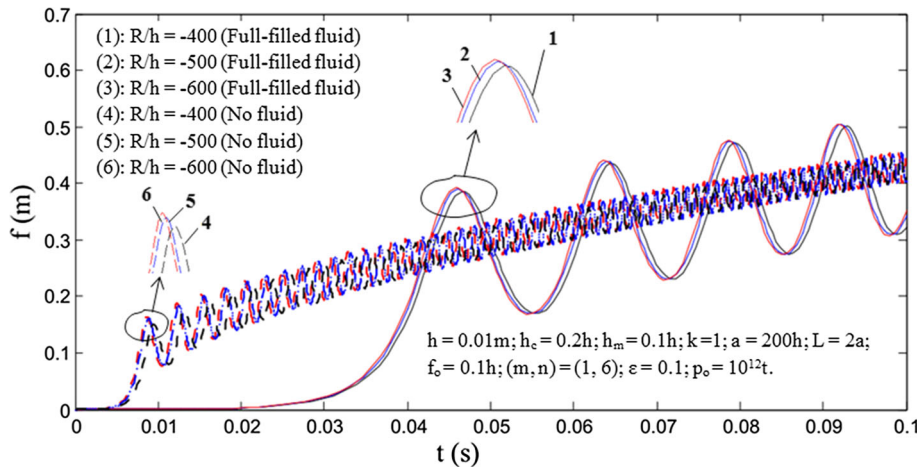


**Fig. 5** Effect of  $R/h$  ratio on dynamical buckling load of imperfect stiffened three-layered concave shells containing full-filled fluid and no fluid under axial compression load

Moreover, when the  $R/h$  ratios increase from 400 to 600, the dynamic critical buckling loads of both shells decrease. The dynamic critical buckling loads of convex shells are higher than those of concave shells with the same parameters and environment. Particularly, with  $R/h = 400$ , the dynamic critical buckling load of the fully-filled convex shell is about  $p_{cr} = 10^{12}t_{cr} = 10^{12}0.045 = 45$  GPa, while the one of the fully-filled concave shell is about  $p_{cr} = 10^{12}t_{cr} = 10^{12}0.04 = 40$  GPa.

**4.2.1.2. Effects of  $L/a$  ratio** Effects of the ratio  $L/a$  on the dynamic buckling load of three-layered convex and concave shells are illustrated in Figs. 6 and 7, respectively. It is observed that when  $L/a$  ratios increase that means the length of shells is increased; the dynamic critical buckling loads of both of shells also rise under axial compression load. The dynamic the critical buckling loads of concave shells, however, always are lower than those of convex shells for both cases: no fluid and fully fluid-filled. For instance, for  $L/a = 4$  with fully filled shells, the dynamical critical buckling load of the convex shell is around  $p_{cr} = 10^{12}t_{cr} = 10^{12}0.08 = 80$  GPa, while the one of the concave shell is around  $p_{cr} = 10^{12}t_{cr} = 10^{12}0.07 = 70$  GPa. Furthermore, the amplitudes as well as the dynamic critical buckling loads of fully fluid-filled shells are always higher than those of shells without fluid.

**4.2.1.3. Effects of  $L/R$  ratio** Based on Figs. 8 and 9, it can be seen that effects of the ratio  $L/R$  on the dynamic buckling of FGM core toroidal shell segments are similar to those of  $L/a$  ratios. Outstandingly, the longer the shells are, the higher the dynamic critical buckling loads of the shells are. There is a special thing that

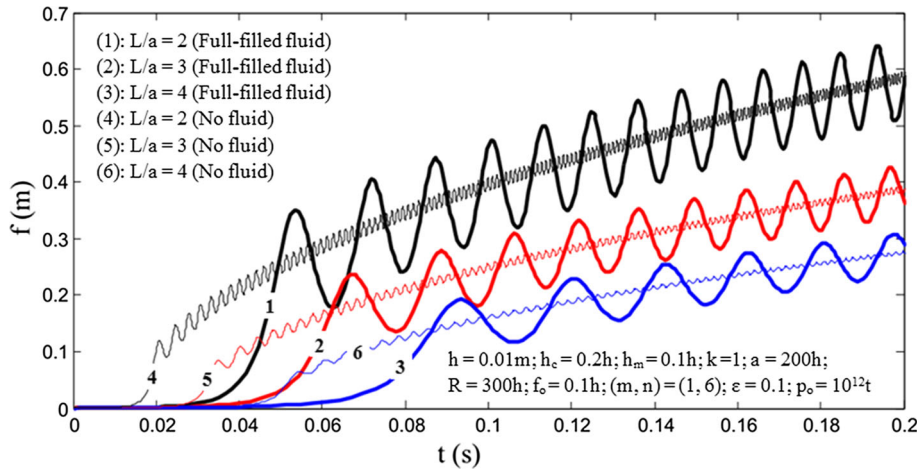


**Fig. 6** Effect of  $L/a$  ratio on dynamical buckling load of imperfect stiffened three-layered convex shells containing full-filled fluid and no fluid under axial compression load

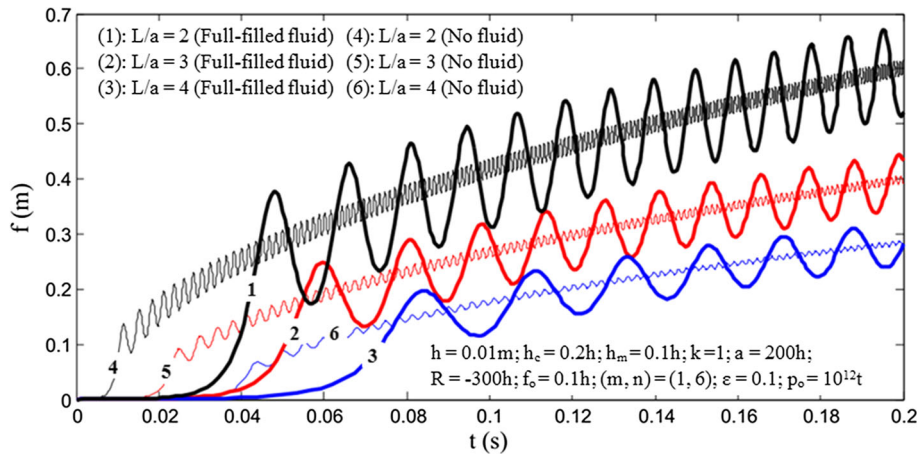


**Fig. 7** Effect of  $L/a$  ratio on dynamical buckling load of imperfect stiffened three-layered concave shells containing full-filled fluid and no fluid under axial compression load

the amplitudes of convex shells always are lower than those of concave shells with the same parameters. This means that the structure of convex shells works better than one of concave shells.

**4.2.1.4. Effects of volume fraction  $k$**  The effect of the volume fraction  $k$  on the dynamical the buckling of the stiffened FGM core convex shell is shown in Fig. 10. The dynamical critical buckling loads of stiffened FGM core toroidal shell segment decrease when the value of the volume fraction index increases. This property apparently appropriates to the real characteristic of the material, since the higher value of  $k$  corresponds to a metal-richer shell which has less stiffness than a ceramic-richer one.

**4.2.1.5. Effects of imperfection** Figures 11 and 12 show effects of imperfection on dynamical buckling loads of stiffened convex and concave shells in full-filled fluid environment, respectively. As can be seen, the imperfection has remarkable influence dynamical buckling loads of structures. For instance, the dynamical critical buckling load of a perfect convex shell is about  $p_{cr} = 10^{12} t_{cr} = 10^{12} 0.075 = 75$  GPa, while the one of an imperfect convex shell with  $f_o = 0.1h$  is about  $p_{cr} = 10^{12} t_{cr} = 10^{12} 0.047 = 47$  GPa. This means that one of perfect convex shell is 1.5 times higher than the one of the imperfect convex shell with  $f_o = 0.1h$ . This is similar to the structure of the concave shell.

**4.2.1.6. Effects of ceramic layer** The effect of the ceramic layer on the dynamic buckling of fully fluid-filled convex shells is illustrated in Fig. 13. The dynamic critical buckling load of FGM core shells increases when the



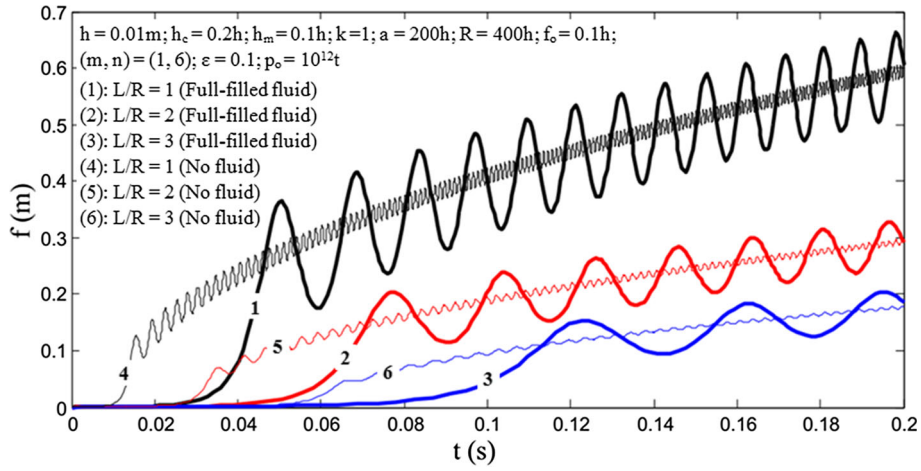


**Fig. 8** Effect of  $L/R$  ratio on dynamical buckling load of imperfect stiffened three-layered convex shells containing full-filled fluid and no fluid under axial compression load

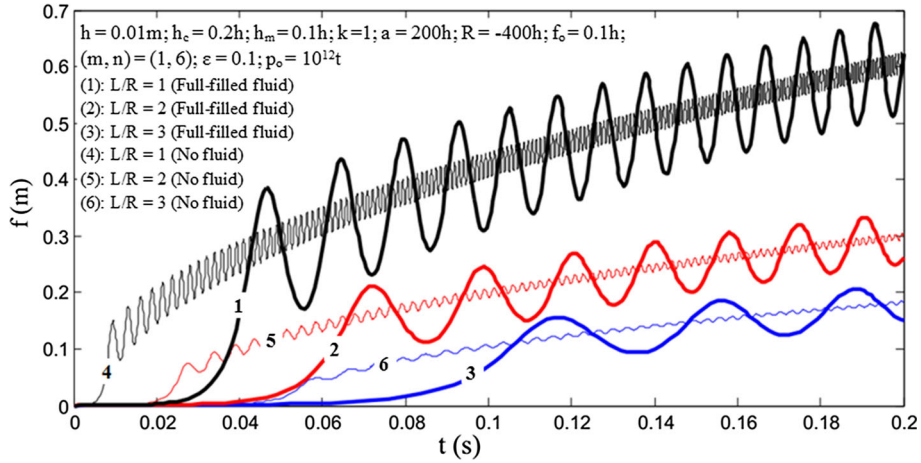


**Fig. 9** Effect of  $L/R$  ratio on dynamical buckling load of imperfect stiffened three-layered concave shells containing full-filled fluid and no fluid under axial compression load

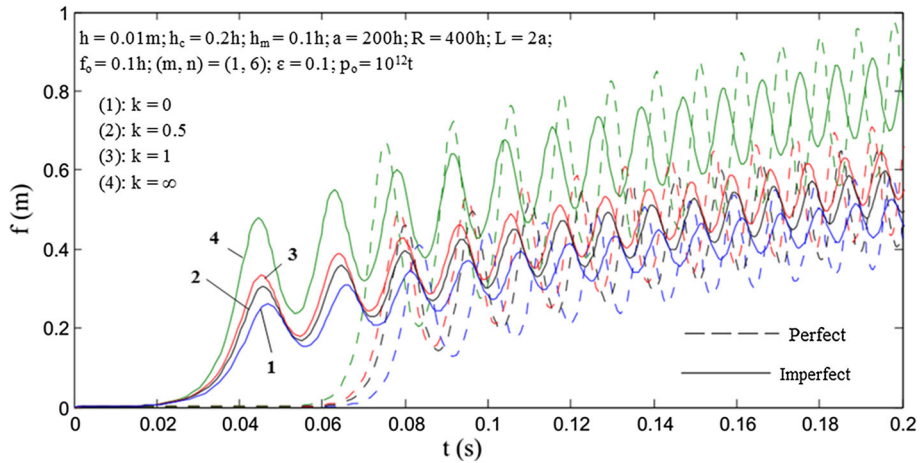


**Fig. 10** Effect of volume fraction  $k$  on dynamical buckling load of perfect and imperfect stiffened three-layered convex shells containing full-filled fluid under axial compression load



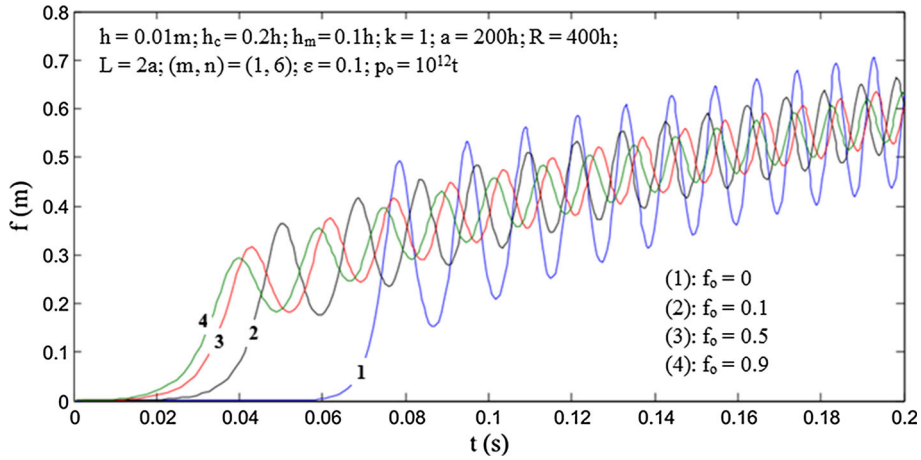


**Fig. 11** Effect of imperfection on dynamical buckling load of imperfect stiffened three-layered convex shells containing full-filled fluid under axial compression load

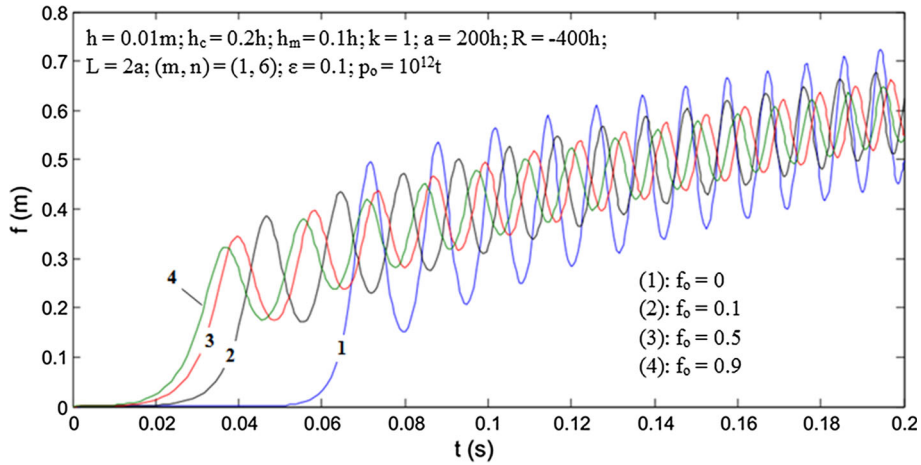


**Fig. 12** Effect of imperfection on dynamical buckling load of imperfect stiffened three-layered concave shells containing full-filled fluid under axial compression load

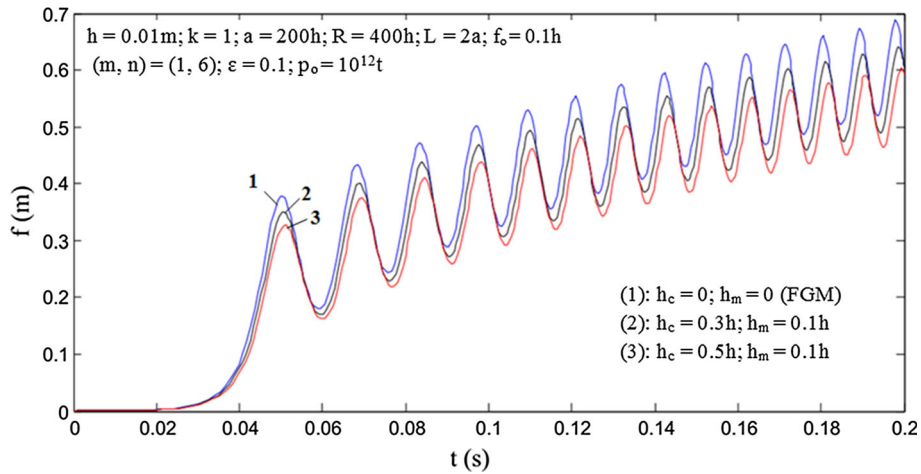


**Fig. 13** Effect of ceramic layer on dynamical buckling load of imperfect three-layered convex shells containing full-filled fluid under axial compression load

**Table 2** Effects of  $L/R$  ratio and  $R/h$  ratio on dynamical critical buckling load (GPa) of imperfect three-layered FGM convex and concave shells under lateral pressure (movable case)

| Shell         | $L/R$ ratio | Environment       | $R/h$ ratio |        |        |
|---------------|-------------|-------------------|-------------|--------|--------|
|               |             |                   | 200         | 300    | 400    |
| Convex shell  | 1           | No fluid          | 0.3984      | 0.5152 | 0.6223 |
|               |             | Full-filled fluid | 1.8555      | 2.0337 | 2.4433 |
|               | 2           | No fluid          | 0.6721      | 0.7698 | 0.7861 |
|               |             | Full-filled fluid | 2.3487      | 3.1698 | 3.6658 |
|               | 3           | No fluid          | 0.7921      | 0.8066 | 0.8097 |
|               |             | Full-filled fluid | 3.1864      | 3.8011 | 4.4064 |
| Concave shell | 1           | No fluid          | 0.3670      | 0.4918 | 0.5875 |
|               |             | Full-filled fluid | 1.8400      | 2.0018 | 2.4198 |
|               | 2           | No fluid          | 0.5280      | 0.6603 | 0.7345 |
|               |             | Full-filled fluid | 2.2912      | 3.0441 | 3.6489 |
|               | 3           | No fluid          | 0.6575      | 0.7354 | 0.7859 |
|               |             | Full-filled fluid | 3.0568      | 3.7818 | 4.2854 |

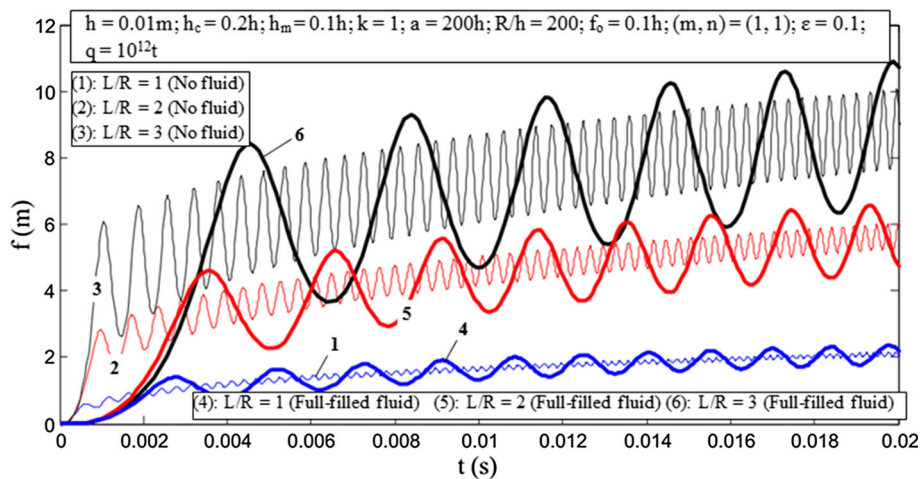


**Fig. 14** Effect of  $L/R$  on dynamical buckling load of imperfect three-layered convex shells containing fluid and no fluid under lateral pressure (movable case)

thickness of ceramic layer increases. It means that the sandwich structures will be stiffer than FGM structures with the same geometry parameters. Moreover, the amplitudes of sandwich structure will be lower than these of FGM structure.

4.2.2 Case 2: Movable case with lateral pressure

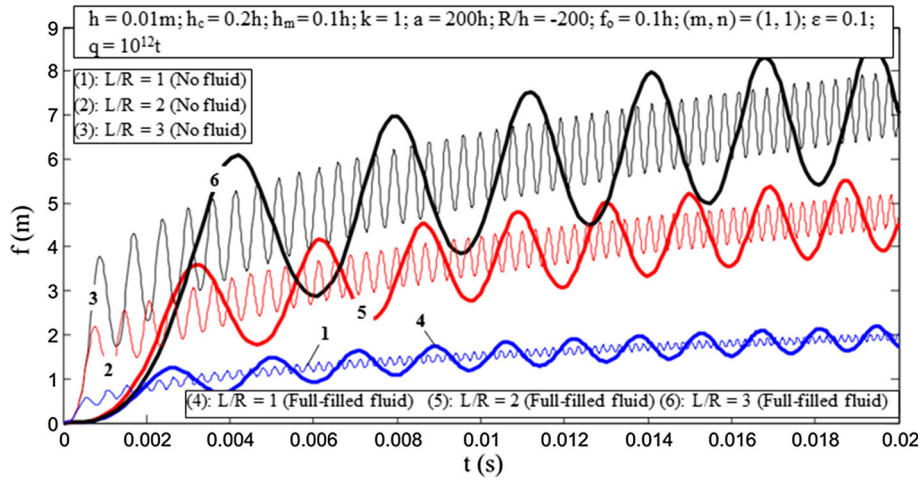
4.2.2.1. Effects of  $R/h$  and  $L/R$  ratio In this section, the paper researches dynamic buckling of three-layered toroidal shell segment under lateral pressure.

Table 2 indicates the effects of  $R/h$  ratio and  $L/R$  ratio on the dynamic buckling of convex shell and concave shell. Figures 14 and 15 express the effect of  $L/R$  ratio on dynamic buckling of convex and concave shell, respectively, in two cases: fully fluid-filled and no fluid. The parameters of the shell are follows:

$$h = 0.01m; h_c = 0.3h; h_m = 0.1h; h_1 = h_2 = d_1 = d_2 = h/2; n_1 = n_2 = 50; a = 100h; f_o = 0.1h; (m, n) = (1, 1); \epsilon = 0.1; q = 10^{12}t.$$

It is observed that the dynamic critical buckling loads of convex and concave shell under lateral pressure will increase if  $R/h$  ratios increase. Furthermore, this also happens to the regulations of  $L/R$  ratios. It means that the longer the shells are, the higher the dynamic critical buckling loads are. On the other hand, the dynamic critical buckling loads of convex shells are always higher than those of concave shells with the same parameters. The dynamic critical buckling loads of full-filled shells are higher about 2.5 to 5 times than those of shells without fluid.

4.2.2.2. Effects of fluid and volume fraction  $k$  Effect of fluid and volume fraction  $k$  on the dynamic critical buckling load of FGM sandwich convex and concave shell subjected to lateral pressure is given in Table 3.



**Fig. 15** Effect of  $L/R$  on dynamical buckling load of imperfect three-layered concave shells containing fluid and no fluid under lateral pressure (movable case)

**Table 3** Effect of volume fraction  $k$  on dynamical critical buckling load (GPa) of imperfect three-layered FGM convex and concave shells under lateral pressure (movable case)

| Shell         | Environment       | $k$    |        |        |        |          |
|---------------|-------------------|--------|--------|--------|--------|----------|
|               |                   | 0      | 0.5    | 1      | 10     | $\infty$ |
| Convex shell  | No fluid          | 0.3763 | 0.3631 | 0.3626 | 0.3611 | 0.3599   |
|               | Full-filled fluid | 1.8151 | 1.8140 | 1.8102 | 1.8099 | 1.8026   |
| Concave shell | No fluid          | 0.3754 | 0.3617 | 0.3591 | 0.3576 | 0.3571   |
|               | Full-filled fluid | 1.7654 | 1.7450 | 1.7357 | 1.8027 | 1.7963   |

$h = 0.01m$ ;  $h_c = 0.3h$ ;  $h_m = 0.1h$ ;  $h_1 = h_2 = d_1 = d_2 = h/2$ ;  $n_1 = n_2 = 50$ ;  $a = 100h$ ;  $R/h = 300$  and  $-300$ ;  $L/a = 2$ ;  $f_o = 0.1h$ ;  $(m, n) = (1, 1)$ ;  $\epsilon = 0.1$ ;  $q = 10^{12}t$

**Table 4** Comparison of dynamical critical buckling load (GPa) of imperfect three-layered FGM convex and concave shells under lateral pressure in two cases without fluid

| R/h                   | 300            |              | 400            |              | 500            |              |
|-----------------------|----------------|--------------|----------------|--------------|----------------|--------------|
|                       | Immovable case | Movable case | Immovable case | Movable case | Immovable case | Movable case |
| $c_2 = 10^{10}$ GPa/s | 0.0132         | 0.0130       | 0.0129         | 0.0127       | 0.0127         | 0.0125       |
| $c_2 = 10^{11}$ GPa/s | 0.0787         | 0.0777       | 0.0782         | 0.0763       | 0.0771         | 0.0758       |
| $c_2 = 10^{12}$ GPa/s | 0.4173         | 0.4153       | 0.4161         | 0.4141       | 0.4153         | 0.4133       |
| R/h                   | -300           |              | -400           |              | -500           |              |
| $c_2 = 10^{10}$ GPa/s | 0.0131         | 0.0129       | 0.0127         | 0.0125       | 0.0125         | 0.0124       |
| $c_2 = 10^{11}$ GPa/s | 0.0762         | 0.0756       | 0.0758         | 0.0753       | 0.0757         | 0.0752       |
| $c_2 = 10^{12}$ GPa/s | 0.4138         | 0.4123       | 0.4113         | 0.4097       | 0.4111         | 0.4094       |

It is apparent that when the volume fraction index increases, this means that metal-richer volume increases, the dynamic critical buckling loads also decrease because of the reduced stiffness of structure. Furthermore, dynamic critical buckling loads of full-filled fluid structures are more around 5.0 times than those of structures without fluid.

**4.2.3 Case 3: Immovable case with lateral pressure**

In this section, dynamic buckling loads of shells with immovable case under lateral pressure are studied.

Tables 4 and 5 describe comparison of dynamical critical buckling loads of imperfect three-layered FGM convex and concave shells in immovable and movable case without fluid and fully-filled with fluid, respectively. The parameters of the problem are as follows:

**Table 5** Comparison of dynamical critical buckling load (GPa) of imperfect three-layered FGM convex and concave shells under lateral pressure in two cases with full-filled fluid

| $R/h$                 | 300            |              | 400            |              | 500            |              |
|-----------------------|----------------|--------------|----------------|--------------|----------------|--------------|
| Loading speed         | Immovable case | Movable case | Immovable case | Movable case | Immovable case | Movable case |
| $c_2 = 10^{10}$ GPa/s | 0.0635         | 0.0629       | 0.0631         | 0.0625       | 0.0627         | 0.0625       |
| $c_2 = 10^{11}$ GPa/s | 0.3630         | 0.3614       | 0.3613         | 0.3597       | 0.3605         | 0.3589       |
| $c_2 = 10^{12}$ GPa/s | 2.0462         | 2.0205       | 1.9901         | 1.9852       | 1.9887         | 1.9801       |
| $R/h$                 | -300           |              | -400           |              | -500           |              |
| $c_2 = 10^{10}$ GPa/s | 0.0628         | 0.0625       | 0.0626         | 0.0624       | 0.0625         | 0.0621       |
| $c_2 = 10^{11}$ GPa/s | 0.3591         | 0.3578       | 0.3553         | 0.3539       | 0.3551         | 0.3537       |
| $c_2 = 10^{12}$ GPa/s | 2.0383         | 2.0147       | 1.9871         | 1.9832       | 1.9862         | 1.9772       |

$h = 0.01\text{m}$ ;  $h_c = 0.3h$ ;  $h_m = 0.1h$ ;  $h_1 = h_2 = d_1 = d_2 = h/2$ ;  $k = 1$ ;  $n_1 = n_2 = 50$ ;  $a = 200h$ ;  $L = 2a$ ;  $f_o = 0.1h$ ;  $(m, n) = (1, 7)$ ;  $\varepsilon = 0.1$ ;  $q = c_2 t$

There are three pivotal comments in the two Tables. Firstly, the dynamic critical buckling loads of both convex and concave shell in the immovable case are higher than those of shells in the movable case. This is explained due to more stiffness of immovable condition. Secondly, the dynamic critical buckling load increases approximately 6.0 times when the loading speed rises 10.0 times. Finally, the regulations of characteristics about the geometry and the environment such as  $R/h$  ratios, convex and concave shell and no fluid and fully fluid-filled are similar to the above-analyzed studies.

## 5 Conclusions

The nonlinear dynamical buckling of imperfect eccentrically stiffened three-layered toroidal shell segments fully-filled with fluid is investigated using the classical shell theory. The Galerkin method, Volmir's assumption and a numerical method using fourth-order Runge–Kutta are computerized for dynamic analysis of shells. Effects of geometrical and material parameters, imperfection and fluid on the nonlinear dynamical buckling behavior of shells are illustrated in the obtained results. Some significant conclusions are obtained as follows:

- The results obtained in this paper are compared with the results of other authors to validate.
- The fluid remarkably influences the dynamic buckling loads of the FGM sandwich toroidal shell segment. Particularly, it makes the dynamical critical buckling loads increase many times more than without fluid.
- Geometrical ratios, imperfection, ceramic and metal layer considerably affect the dynamical buckling behavior of shells. Furthermore, the dynamic critical buckling loads of a concave shell are always lower than those of a convex shell with the same parameters. It means that the carrying capacity of a convex shell is better than that of a concave shell.
- The dynamical critical buckling pressure loads of shells in the immovable case are always greater than those of shells in the movable case.

**Acknowledgements** This work was supported by The scientific research Project of Hanoi University of Science and Technology under Grant number T2016-PC-056. The authors are grateful for this support.

## References

1. Chen, W.Q., Bian, Z.G., Ding, H.J.: Three-dimensional vibration analysis of fluid-filled orthotropic FGM cylindrical shells. *Int. J. Mech. Sci.* **46**, 159–171 (2004)
2. Khorshidi, K., Bakhsheshy, A.: Free vibration analysis of a functionally graded rectangular plate in contact with a bounded fluid. *Acta Mech.* **226**, 3401–3423 (2015)
3. Sheng, G.G., Wang, X.: Thermomechanical vibration analysis of a functionally graded shell with flowing fluid. *Eur. J. Mech. A Solids* **27**, 1075–1087 (2008)
4. Bochkarev, S.A., Matveenko, V.P.: Numerical analysis of stability of a stationary or rotating circular cylindrical shell containing axially flowing and rotating fluid. *Int. J. Mech. Sci.* **68**, 258–269 (2013)
5. Ross, C.T.F., Koster, P., Little, A.P.F., Tewkesbury, G.: Vibration of a thin-walled prolate dome under external water pressure. *Ocean Eng.* **34**, 560–575 (2007)

6. Prado, Z., Goncalves, P.B., Paidoussis, M.P.: Non-linear vibrations and instabilities of orthotropic cylindrical shells with internal flowing fluid. *Int. J. Mech. Sci.* **52**, 1437–1457 (2010)
7. Zhu, X., Ye, W.B., Li, T.Y., Chen, C.: The elastic critical pressure prediction of submerged cylindrical shell using wave propagation method. *Ocean Eng.* **58**, 22–26 (2013)
8. Sburlati, R.: An axisymmetric elastic analysis for circular sandwich panels with functionally graded cores. *Compos. Part B Eng.* **43**, 1039–1044 (2012)
9. Sofiyev, A.H., Kuruoglu, N.: Dynamic instability of three-layered cylindrical shells containing an FGM interlayer. *Thin Walled Struct.* **93**, 10–21 (2015)
10. Sofiyev, A.H., Hui, D., Najafov, A.M., Turkaslan, S., Dorofeyskaya, N., Yuan, G.Q.: Influences of shear stresses and rotary inertia on the vibration of functionally graded coated sandwich cylindrical shells resting on the Pasternak elastic foundation. *J. Sandw. Struct. Mater.* (2015). doi:10.1177/1099636215594560
11. Alibeigloo, A., Alizadeh, M.: Static and free vibration analyses of functionally graded sandwich plates using state space differential quadrature method. *Eur. J. Mech. A Solids* **54**, 252–266 (2015)
12. Taibi, F.Z., Benyoucef, S., Tounsi, A., Bouiadjra, R.B., Bedia, E.A.A., Mahmoud, S.R.: A simple shear deformation theory for thermo-mechanical behavior of functionally graded sandwich plates on elastic foundation. *J. Sandw. Struct. Mater.* **17**, 99–129 (2015)
13. Xia, X., Shen, H.S.: Vibration of post-buckled sandwich plates with FGM face sheets in a thermal environment. *J. Sound Vib.* **314**, 254–274 (2008)
14. Khalili, S.M.R., Mohammadi, Y.: Free vibration analysis of sandwich plates with functionally graded face sheets and temperature-dependent material properties: A new approach. *Eur. J. Mech. A Solids* **35**, 61–74 (2012)
15. Wang, Z., Shen, H.S.: Nonlinear dynamic response of sandwich plates with FGM face sheets resting on elastic foundations in thermal environments. *Ocean Eng.* **57**, 99–110 (2013)
16. Shariyat, M.: Dynamic thermal buckling of suddenly heated temperature-dependent FGM cylindrical shells, under combined axial compression and external pressure. *Int. J. Solids Struct.* **45**, 2598–2612 (2008)
17. Shariyat, M.: Dynamic buckling of suddenly loaded imperfect hybrid FGM cylindrical shells with temperature-dependent material properties under thermo-electro-mechanical loads. *Int. J. Mech. Sci.* **50**, 1561–1571 (2008)
18. Huang, H., Han, Q.: Nonlinear dynamic buckling of functionally graded cylindrical shells subjected to time-dependent axial load. *Compos. Struct.* **92**, 593–598 (2010)
19. Huang, H., Han, Q.: Research on nonlinear postbuckling of functionally graded cylindrical shells under radial loads. *Compos. Struct.* **92**, 1352–1357 (2010)
20. Bich, D.H., Dung, D.V., Nam, V.H., Phuong, N.T.: Nonlinear static and dynamic buckling analysis of imperfect eccentrically stiffened functionally graded circular cylindrical thin shells under axial compression. *Int. J. Mech. Sci.* **74**, 190–200 (2013)
21. Bich, D.H., Dung, D.V., Hoa, L.K.: Nonlinear static and dynamic buckling analysis of functionally graded shallow spherical shells including temperature effects. *Compos. Struct.* **94**, 2952–2960 (2012)
22. Sofiyev, A.H., Kuruoglu, N.: Domains of dynamic instability of FGM conical shells under time dependent periodic loads. *Compos. Struct.* **136**, 139–148 (2016)
23. Sofiyev, A.H.: On the dynamic buckling of truncated conical shells with functionally graded coatings subject to a time dependent axial load in the large deformation. *Compos. Part B Eng.* **58**, 524–533 (2014)
24. Duc, N.D., Quan, T.Q., Luat, V.D.: Nonlinear dynamic analysis and vibration of shear deformable piezoelectric FGM double curved shallow shells under damping-thermo-electro-mechanical loads. *Compos. Struct.* **125**, 29–40 (2015)
25. Zhang, J., Li, S.: Dynamic buckling of FGM truncated conical shells subjected to non-uniform normal impact load. *Compos. Struct.* **92**, 2979–2983 (2010)
26. McElman, J.A.: Eccentrically stiffened shallow shells of double curvature. NASA Technical note; D-3826 (1967)
27. Hutchinson, J.W.: Initial post-buckling behavior of toroidal shell segments. *J. Solid Struct.* **3**, 97–115 (1967)
28. Stein, M., McElman, J.A.: Buckling of segments of toroidal shells. *AIAA J.* **3**, 1704–1709 (1965)
29. Bich, D.H., Ninh, D.G., Thinh, T.I.: Buckling analysis of eccentrically stiffened functionally graded toroidal shell segments under mechanical load. *J. Eng. Mech. ASCE* **142**, 0405054-1–0405054-10 (2015)
30. Bich, D.H., Ninh, D.G.: Post-buckling of sigmoid-functionally graded material toroidal shell segment surrounded by an elastic foundation under thermomechanical loads. *Compos. Struct.* **138**, 253–263 (2016)
31. Bich, D.H., Ninh, D.G., Thinh, T.I.: Nonlinear buckling analysis of FGM toroidal shell segments filled inside by an elastic medium under external pressure loads including temperature effects. *Composite: Part B. Engineering* **87**, 75–91 (2016)
32. Ninh, D.G., Bich, D.H., Kien, B.H.: Torsional buckling and post-buckling behaviors of eccentrically stiffened functionally graded toroidal shell segments surrounded by an elastic medium. *Acta Mech.* **226**, 3501–3519 (2015)
33. Ninh, D.G., Bich, D.H.: Nonlinear buckling of eccentrically stiffened functionally graded toroidal shell segments under torsional load surrounded by elastic foundation in thermal environment. *Mech. Res. Commun.* **72**, 1–15 (2016)
34. Ninh, D.G., Bich, D.H.: Nonlinear thermal vibration of eccentrically stiffened ceramic-FGM-metal layer toroidal shell segments surrounded by elastic foundation. *Thin Walled Struct.* **104**, 198–210 (2016)
35. Brush, D.O., Almorh, B.O.: Buckling of Bars, Plates and Shells. Mc. Graw-Hill, New York (1975)
36. Volmir, A.S.: Nonlinear Dynamic of Plates and Shells, science edition (1972) (in Russian)
37. Budiansky, B., Roth, R.S.: Axisymmetric dynamic buckling of clamped shallow spherical shells. NASA Technical Note D-510, pp. 597–609 (1962)